EVAPORATIVE COOLING OF CONTINUOUSLY DRAWN GLASS FIBERS BY WATER SPRAYS

Matthew Sweetland
John H. Lienhard V

W.M. Rohsenow Heat and Mass Transfer Laboratory
Department of Mechanical Engineering
Massachusetts Institute of Technology
77 Massachusetts Avenue, Rm 3-162
Cambridge MA 02139-4307 USA

Abstract

This paper examines the effect of the water sprays commonly used to cool freshly drawn glass fibers. A model has been developed using a Karman-Pohlhausen treatment of the velocity and thermal boundary layers and accounting for the evaporation of an entrained water spray. Solutions of the model equations have been calculated, and the effect of changing various process parameters is studied. Variations in Sauter mean diameter, spray density, and spray placement along the fiber are considered, as well as the effect of fiber diameter and drawing speed. Fiber temperature profiles for different values of the process variables are presented.

International Journal of Heat and Mass Transfer, **43** (2000) 777-790.

Nomenclature

Symbol	Description
a	fiber radius [m]
$a_1,\ a_2,\ a_3$	β series expansion coefficients for small α
A_1	k_{evap} curve-fit coefficient [m^2/sK^2]
B	$(k\rho c_p)/(k_f \rho_f c_{p_f})$
B_1	k_{evap} curve-fit coefficient [m^2/sK]
C_1	k_{evap} curve-fit coefficient [m^2/s]
c_p	air specific heat capacity [J/kgK]
c_{p_f}	fiber specific heat capacity [J/kgK]
D_0	initial droplet diameter [m]
D	droplet diameter [m]
h_{fg}	latent heat of vaporization [J/kg]
k	air thermal conductivity [W/m·K]
k_f	fiber thermal conductivity [W/m·K]
k_{evap}	evaporation coefficient [m^2/s]
$\dot{m}'''$	local volumetric evaporation rate [kg/m^3s]
n_o	environmental spray density [drops/m^3]
n	boundary layer spray density [drops/m^3]
Pr	Prandtl number
Q	convective heat flow from fiber [W]
$\dot{q}_e$	volumetric heating due to vaporization [W/m^3]
t	time [s]
T	boundary layer air temperature [K]
T_e	environmental air temperature [K]
T_f	fiber temperature [K]
u	axial boundary layer velocity [m/s]
U	fiber velocity [m/s]
v	radial boundary layer velocity [m/s]
x	axial distance from bushing plate [m]
X	$x\nu/Ua^2$
y	radial distance from fiber surface [m]

Greek Symbols

α	velocity profile parameter
β	temperature profile parameter
δ	momentum boundary layer thickness [m]
δ_T	thermal boundary layer thickness [m]
η	dimensionless volumetric energy ratio, $(\rho c_p)/(\rho_f c_{p_f})$
Θ	boundary layer air temperature defect [K]
Θ_f	fiber temperature defect [K]
μ	dynamic viscosity [kg/m·s]
ν	kinematic viscosity [m^2/s]
ρ	air density [kg/m^3]
ρ_f	fiber density [kg/m^3]
ρ_w	water density [kg/m^3]

Introduction

Glass fibers are used for reinforcement of products ranging from structural plastics to fabrics. Such fibers are made by drawing molten glass through an array of small diameter bushings. The glass solidifies within a few centimeters of the bushing and is then pulled a distance of one to two meters prior to coating with various binders or sizing compounds. Typical fiber diameters are 5-30 μm with drawing speeds varying from 15-90 m/sec and array sizes ranging from several hundred to several thousand fibers. This process has been in use for several decades [1].

The cooling of the fibers from the glass extrusion temperature (1500 K) to a temperature where the coatings can be applied (below 365 K) is a rate limiting step. The high fiber speeds and short drawing lengths require a temperature drop of over 1100 K in roughly 25 ms. In order to enhance the heat removal from the fibers, the fiber bundle is sprayed with water from atomizing nozzles. Typical Sauter mean droplet diameters are on the order of 15 to 20 μm and droplet number densities may range from a few hundred per cm^3 to a few thousand per cm^3, depending upon nozzle and airflow conditions. At the fiber temperatures involved, water cannot wet the fiber surface without an initial quenching process. Moreover, at typical number densities, droplet speeds, and fiber speeds, direct collisions of droplets with the fibers are infrequent and will involve only a small percentage of the fiber surface. Thus, for most of the fiber, cooling enhancement is evidently due primarily to evaporative effects in the air adjacent to the fibers.

At present, no quantitative method is available for calculating the effect of the water spray on the cooling rate of the fibers. Production stations have been designed through a trial and error process in nozzle placement and operating conditions. Determining the effects of changing process parameters, such as spray size and density, is only possible through direct experimentation on production systems, which is both time consuming and expensive. A model is needed to calculate the effects of evaporative cooling on the manufacturing process. Such a model can be used for improvement of the existing process and as a design tool for developing new processes and products.

The basic problem of boundary layer growth and heat transfer from continuous cylinders moving through a still fluid has been studied quite extensively. Early work by Seban and Bond [2] and Glauert and Lighthill [3] examined stationary cylinders in a moving fluid. Sakiadis

[4] showed that the case of a moving cylinder in stationary fluid leads to different flow and temperature fields; he developed a momentum integral solution for the boundary layer flow around a moving cylinder using a logarithmic velocity profile. These integral solutions have been used in many subsequent studies [5,6,7,8], and exact solutions of the boundary layer equations by Sayles [9] lie within 9% of the integral solutions. Convection from isothermal fibers was studied using integral results by Bourne and Elliston [5], assuming constant fluid properties; exact solutions were obtained by Karniš and Pechoč [8] and were found to lie within 10% of the integral results. In addition, Beese and Gersten [10] have provided perturbation solutions for isothermal fibers that are valid in the limit of large fiber diameter.

Of greatest relevance to our case are those studies that account for the finite heat capacity and axial temperature drop of the fibers. Bourne and Dixon [6] used integral solutions for the cooling fiber, neglecting conduction resistance within the fiber and using averaged values of the fluid properties. Their results showed good agreement with experimental measurements by Arridge and Prior [11] and by Alderson et al. [12] on 15 to 50 μm diameter on glass fibers. They showed that attention to the averaging of temperature-dependent air properties was quite important. Chida and Katto [7] subsequently amended the Bourne and Dixon theory to account for radial heat conduction in the fibers; for conditions typical of glass fibers, radial conduction proves to be negligible. Chida and Katto also developed scaling parameters for the problem which were shown to collapse the above mentioned experiments. Maddison and McMillan [13] reported further experiments on fiber cooling which were in general agreement with the results of Arridge and Prior. Kang et al. [14] performed experiments on large diameter aluminum cylinders drawn through air and water; they found good agreement with the scaled theoretical results of Chida and Katto. Richelle et al. [15] provided exact solutions of the boundary layer equations for moving fibers. Roy Chaudhury and Jaluria [16] performed numerical integrations of the full elliptic equations and found agreement with the experimental studies that was similar to that of Chida and Katto. Together, these studies provide strong validation of the integral theory originally developed by Bourne and Dixon.

These studies focus on laminar flow in the boundary layers; at present, little is known about the stability of these boundary layers. Several of the above studies [5,8,10,15], and others [17,18], have also produced results for the Nusselt number of fibers moving through dry air.

We are aware of no work addressing spray cooling of glass fibers, although a large body of work deals with other problems in spray cooling. Such studies include cooling of atomized flu-

ids [19], cooling of large flat surfaces [20,21] through direct spray impingement on the surface, and cooling of air by water spray [22,23]. A recent study by Buckingham and Haji-Sheikh [24] considered spray cooling of large metal cylinders. Of particular relevance is their identification of a convection-dominated cooling regime in which water spray was found to evaporate within the boundary layer of a high temperature surface, without actually impinging upon it. This process is quite similar to the one modeled here for glass fibers.

In this paper, we use the Karman-Pohlhausen integral method to develop a set of equations that describe the growth of the fiber thermal boundary layer with droplet evaporation occurring in the boundary layer. In the limit of no spray, our approach is identical to the Bourne and Dixon theory [6], although we have not assumed constant fluid properties along the length of the fiber. The boundary layer evaporation term is evaluated using a single droplet model, and the resulting equations are used to calculate fiber temperature profiles for various spray and fiber conditions. The fiber is assumed to travel through undisturbed ambient air within which the spray is uniformly distributed. We assume throughout this study that the droplets are dispersed in the boundary layer and do not directly interact with the fiber (*e.g.*, through some type of collision and film boiling process). We further assume that the boundary layer remains laminar and that crossflows are unimportant. Radiation cooling of small diameter, high speed fibers is easily shown to be small relative to forced convective cooling, and it is not included here.

Development of Boundary Layer Evaporation Model

The boundary layer equations in cylindrical coordinates for laminar, steady state, incompressible flow on a continuous moving fiber in still air are

$$\frac{\partial u}{\partial x} + \frac{\partial v}{\partial y} + \frac{v}{a+y} = 0 \tag{1}$$

$$\rho u \frac{\partial u}{\partial x} + \rho v \frac{\partial u}{\partial y} = \mu \left(\frac{\partial^2 u}{\partial y^2} + \frac{1}{a+y} \frac{\partial u}{\partial y} \right) \tag{2}$$

$$u \frac{\partial T}{\partial x} + v \frac{\partial T}{\partial y} = \frac{k}{\rho c_p (a+y)} \frac{\partial}{\partial y} \left((a+y) \frac{\partial T}{\partial y} \right) + \frac{1}{\rho c_p} \dot{q}_e \tag{3}$$

where u is the axial velocity, v is the radial velocity, $\dot{q}_e$ is a volumetric heat source due to evaporation (W/m^3), y is measured from the fiber surface, and the coordinate system is further

described in Fig. 1. The position $y = 0$ corresponds to the fiber surface and $x = 0$ to the fiber bushing plate. The fiber radius and fiber velocity are assumed constant over the length of the fiber[1]. All equations are written in terms of y rather than r to simplify the boundary conditions. Equations (1) and (2) are subject to the boundary conditions

$$u = U, v = 0 \text{ at } y = 0 \tag{4}$$

$$u \to 0, v \to 0 \text{ as } y \to \infty \tag{5}$$

where U is the fiber speed, and equation (3) is subject to the boundary conditions

$$T(x, y) = T_f(x) \text{ at } y = 0 \tag{6}$$

$$T(x, y) \to T_\infty, \ \frac{\partial T}{\partial y} \to 0 \text{ as } y \to \infty \tag{7}$$

where $T_f(x)$ is the local fiber temperature. An additional boundary condition on equation (3) is $\dot{q}_e \big|_{y=0} = 0$. This condition arises from the assumption that no drops touch the surface of the fiber.

Following the work of Glauert and Lighthill [3] for axial flow over a long cylinder and the analyses of a continuous cylinder moving through a still fluid by Sakiadis and others [4,8], an approximate velocity profile of the form

$$\frac{u}{U} = 1 - \frac{1}{\alpha} \ln(1 + \frac{y}{a}) \text{ for } y \le \delta(x) \tag{8}$$

$$\frac{u}{U} = 0 \text{ for } y \ge \delta(x) \tag{9}$$

is assumed, where α is a function of x only, and the spray is assumed to have negligible effect on the velocity boundary layer. (The number density of spray is relatively low and the typically boundary layer thicknesses on long thin fibers are many times greater than typical droplet diameters.) By setting $u/U = 0$, the boundary layer thickness δ, can be defined as $\delta = a(e^\alpha - 1)$. As shown by Bourne and Elliston [5], an integral analysis of equations (1) and (2) allows the relationship of the velocity profile parameter, α, to x to be evaluated as

$$\frac{2\nu x}{U a^2} = \frac{e^{2\alpha} - 1}{\alpha} + \mathrm{Ei}(2\alpha) + \ln(2\alpha) + \gamma - 2 \tag{10}$$

[1]The short necking region is neglected.

where $\gamma = .5572\ldots$ is Euler's constant and $\mathrm{Ei}(2\alpha)$ is the exponential integral. Note that equation (10) shows α to be a function of the parameter $X = \nu x/Ua^2$.

To obtain a corresponding equation for the temperature profile in the presence of evaporation, we consider the boundary layer control volume shown in Fig. 2. Neglecting conduction in the x direction, an energy balance yields

$$\frac{d}{dx}\int_0^\infty \rho c_p T(x,y)u(x,y)\,2\pi(a+y)dy\,\Delta x = -2\pi ak\left.\frac{\partial T}{\partial y}\right|_{y=0}\Delta x + \int_0^\infty \dot{q}_e\,2\pi(a+y)dy\,\Delta x \quad (11)$$

where $u(x,y)$ is the boundary layer velocity profile, $T(x,y)$ is the boundary layer temperature profile and k is the thermal conductivity of the air.

Another equation is needed to determine the axial variation in fiber temperature. For fibers with diameters less than 200 μm, Papamichael and Miaoulis [25] have shown that the effect of axial conduction can be neglected. The analysis of Chida and Katto [7] shows that radial conduction depends upon the parameter $B = (k\rho c_p)/(k_f\rho_f c_{p_f})$; for glass fibers drawn through air, B is on the order of 1.6×10^{-5}, and radial conduction may be ignored. Using a control volume on a section of the fiber (Fig. 3), energy conservation for the fiber is described by

$$\frac{d}{dx}\left(\pi a^2\rho_f c_{p_f}T_f U\right) = 2\pi ak\left.\frac{\partial T}{\partial y}\right|_{y=0} \quad (12)$$

where ρ_f is the fiber density, c_{p_f} is the fiber specific heat, and conduction along and across the fiber is neglected. Defining the temperature defects

$$\Theta(x,y) = T(x,y) - T_\infty \quad \text{and} \quad \Theta_f(x) = T_f(x) - T_\infty \quad (13)$$

a temperature distribution similar to the velocity distribution can be assumed [6]

$$\frac{\Theta}{\Theta_f} = 1 - \frac{1}{\beta}\ln\left(1+\frac{y}{a}\right) \quad \text{for} \quad y \le \delta_T \quad (14)$$

$$\frac{\Theta}{\Theta_f} = 0 \quad \text{for} \quad y \ge \delta_T$$

where β is a function of x. This form of temperature profile is acceptable in so far as the evaporative term in equation (3) is smaller than the others and acts to thin the boundary layer over some distance in x, while having a small influence on the local shape in y. Evaporative

effects will modify the evolution of β with x. Rearranging equation (12) and substituting for the assumed temperature profile yields

$$\frac{a\rho_f c_{p_f} U}{2}\frac{d\Theta_f}{dx} = \frac{-k\Theta_f}{\beta a} \tag{15}$$

which describes the decay of the fiber temperature.

After substituting for the velocity and temperature profiles and evaluating the integral on the lefthand side of equation (11) with the assumption $\delta \le \delta_T$, the equation becomes

$$\frac{d}{dx}\left[\frac{1}{4}\frac{a^2\Theta_f U e^{2\alpha}(1-\alpha+\beta)}{\alpha\beta} - \frac{1}{4}\frac{a^2\Theta_f U(2\alpha\beta+\alpha+1+\beta)}{\alpha\beta}\right] = \frac{-k}{\rho c_p}\left(\frac{-\Theta_f}{\beta}\right) + \frac{1}{\rho c_p}\int_0^{\delta_T}\dot{q}_e(a+y)dy. \tag{16}$$

Expanding the lefthand side of equation (16) leads to an expression in $d\alpha/dx$, $d\Theta_f/dx$ and $d\beta/dx$, which can be simplified by using equation (15) to eliminate $d\Theta_f/dx$ and by using

$$\frac{d\alpha}{dx} = \frac{2\nu\alpha^2}{Ua^2\left(-e^{2\alpha}+\alpha e^{2\alpha}+\alpha+1\right)} \tag{17}$$

(from equation 10) to eliminate $d\alpha/dx$ and to transform $d\beta/dx$ to $d\beta/d\alpha$. A differential equation for β is obtained

$$\frac{d\beta}{d\alpha} = \frac{2\beta}{\alpha\,\mathrm{Pr}} + \frac{\eta}{\alpha^2\,\mathrm{Pr}}\left(e^{2\alpha}-\alpha e^{2\alpha}+\beta e^{2\alpha}-2\alpha\beta-\alpha-1-\beta\right) - \frac{\beta}{\alpha}\frac{\left(2\alpha e^{2\alpha}-2\alpha^2 e^{2\alpha}+2\alpha\beta e^{2\alpha}-e^{2\alpha}-\beta e^{2\alpha}+1+\beta\right)}{\left(-e^{2\alpha}+\alpha e^{2\alpha}+\alpha+1\right)} + \frac{2\beta^2}{\Theta_f\alpha k\mathrm{Pr}}\int_0^{\delta_T}\dot{q}_e(a+y)dy \tag{18}$$

where Pr is the Prandtl number and $\eta = (\rho c_p)/(\rho c_p)_f$; in the absence of evaporative cooling, $\beta = \beta(X, \mathrm{Pr}, \eta)$.

This result is correct as long as the velocity boundary layer δ is smaller than the thermal boundary layer δ_T, which is the normal case for a Prandtl number less than unity. With the addition of spray, however, the thermal boundary layer will actually start to shrink until the thermal boundary layer will be fully contained by the velocity boundary layer. When this happens, the integration across the boundary layer of equation (11) is evaluated from 0 to $\delta_T = a(e^{\beta}-1)$ rather than 0 to $\delta = a(e^{\alpha}-1)$. Using the same method as used to develop equation (18), the

differential equation for β becomes

$$\frac{d\beta}{d\alpha} = \frac{-2\alpha\beta}{\mathrm{Pr}}\left[\frac{\left(2\frac{e^{2\alpha}}{\alpha} - \frac{e^{2\alpha}-1}{\alpha^2} - \frac{e^{2\alpha}}{\alpha} + \frac{1}{\alpha}\right)}{(-2\beta e^{2\beta} - 2\alpha\beta e^{2\beta} + 2\beta^2 e^{2\beta} + e^{2\beta} + \alpha e^{2\beta} - \alpha - 1)}\right]$$
$$- \frac{2\alpha\beta^2}{\Theta_f k\mathrm{Pr}}\left[\frac{\left(2\frac{e^{2\alpha}}{\alpha} - \frac{e^{2\alpha}-1}{\alpha^2} - \frac{e^{2\alpha}}{\alpha} + \frac{1}{\alpha}\right)}{(-2\beta e^{2\beta} - 2\alpha\beta e^{2\beta} + 2\beta^2 e^{2\beta} + e^{2\beta} + \alpha e^{2\beta} - \alpha - 1)}\right]\int_0^{\delta_T} \dot{q}_e\,(a+y)dy$$
$$+ \frac{\eta}{\mathrm{Pr}}\left(-e^{2\beta} - \alpha e^{2\beta} + \beta e^{2\beta} + 2\alpha\beta + \alpha + 1 + \beta\right)$$
$$\times\left[\frac{\left(2\frac{e^{2\alpha}}{\alpha} - \frac{e^{2\alpha}-1}{\alpha^2} - \frac{e^{2\alpha}}{\alpha} + \frac{1}{\alpha}\right)}{(-2\beta e^{2\beta} - 2\alpha\beta e^{2\beta} + 2\beta^2 e^{2\beta} + e^{2\beta} + \alpha e^{2\beta} - \alpha - 1)}\right]$$
$$+ \frac{\beta}{\alpha}\frac{\left(-e^{2\beta} + \beta e^{2\beta} + 1 + \beta\right)}{(-2\beta e^{2\beta} - 2\alpha\beta e^{2\beta} + 2\beta^2 e^{2\beta} + e^{2\beta} + \alpha e^{2\beta} - \alpha - 1)}. \quad (19)$$

The presence of Θ_f in equations (18) and (19) prevents direct integration of β with α. In addition, the evaporation term will be shown to be a function of Θ_f. Equations (18) and (19) can be used to evaluate the change in the thermal boundary layer due to normal boundary layer growth and due to evaporation within the boundary layer. The value of β can be evaluated as a function of α which in turn can be used to evaluate the fiber position. Knowledge of the thermal boundary layer at any point on the fiber can then be used to evaluate the heat transfer from the fiber to the surroundings.

Modeling Evaporation

Our aim is to evaluate the evaporation integrals in equations (18) and (19). We do this by calculating the total evaporation rate in successive differential control volumes of length Δx along the fiber; axial variations in the evaporation are accounted for in the subsequent numerical integration of the equations in x. The evaporation rate in the increment Δx is proportional to the total droplet surface area and a temperature-dependent evaporation coefficient. The total droplet surface area, in turn, depends upon the droplet size distribution and number density. For evaporation, the droplet size distribution is best described using the Sauter mean diameter (SMD), which is the diameter of a drop having the average surface area to volume ratio of the entire spray cloud.

Several approximations are made in modeling the droplet evaporation, the justification for which is discussed in detail in [26]. The transient warm-up time of each drop presumed short compared to droplet lifetime: the droplets quickly reach the wet-bulb temperature appropriate to the local boundary layer air temperature and humidity. The droplets in the boundary layer are assumed to be fully entrained and to travel at the air velocity corresponding to the radial position of the center of the drop. The droplets in the boundary layer never touch the fiber surface while fiber temperature is above the droplet saturation temperature; the solutions obtained apply only to this nonwetting regime. The droplets in the boundary layer are assumed to be uniform at the Sauter mean diameter.

A well-established formula exists for the evaporation rate of a single droplet [27]:

$$D^2 = D_0^2 - k_{evap}t \tag{20}$$

where D is the droplet diameter at time t, D_0 is the original droplet diameter, and k_{evap} is an evaporation constant that is dependent on temperature and relative humidity and which can be calculated using mass transfer theory [28]. The coefficient k_{evap} was calculated for a temperature range from 300 K to 1500 K using both low and high rate mass transfer theory, and the resulting data were fit to second-order polynomial expressions of the form

$$k_{evap} = A_1 T^2 + B_1 T + C_1 \tag{21}$$

where T is the local air temperature, which will vary with position y across the thickness of the boundary layer and with distance x along the fiber. The air is assumed to have zero relative humidity, giving an upper bound on the cooling effect. Evaluation of the total mass evaporated, after integration of our equations, shows that axial increases in the relative humidity of air in the boundary layer produce no more than a 4% decrease in the evaporation rate, and generally much less than that. We have therefore neglected the effect of axial changes in the relative humidity.

Within an annular section of the differential control volume, the volumetric evaporative heat loss is simply the latent heat of vaporization at droplet temperature, h_{fg}, times the mass evaporation rate per unit volume, $\dot{m}'''$ (kg/m^{3}s), evaluated locally. Thus, the evaporative cooling rate of the boundary layer increment can be expressed as an integral through the radial thickness of the boundary layer:

$$\int_0^{\delta_T} \dot{q}_e \, 2\pi(a+y)dy\,\Delta x = \int_0^{\delta_T} h_{fg}\dot{m}''' \, 2\pi(a+y)dy\,\Delta x. \tag{22}$$

The evaporation rate is the time rate of change of the mass of droplets per unit volume:

$$\dot{m}''' = \frac{d}{dt}\left(n\,\rho_w\frac{\pi}{6}D^3\right) = u(x,y)\frac{d}{dx}\left(n\,\rho_w\frac{\pi}{6}D^3\right) = u(x,y)\,\rho_w\frac{\pi}{6}\left(D^3\frac{dn}{dx} + n\frac{dD^3}{dx}\right) \quad (23)$$

for n the local number density (droplets per m^3), D the Sauter mean diameter of the spray, and $u(x,y)$ the local air speed.

In order to satisfy the condition that no droplets touch the fiber, a linear droplet density distribution is assumed near the fiber

$$n = \frac{n_0 y}{\delta} \quad (24)$$

where n_0 is the droplet density outside the boundary layer and δ is the local boundary layer thickness[2]. The number density, n_0, is assumed to be independent of x after the point where spraying is initiated; the spray is also assumed to have a uniform angular distribution about the fiber. The evaporation rate can now be written with equation (8) as

$$\dot{m}''' = \frac{\pi\rho_w n_0 y}{2\delta}\left[U - \frac{U}{\alpha}\ln\left(1+\frac{y}{a}\right)\right]D^2\frac{dD}{dx} \quad (25)$$

where the term dD/dx can be evaluated with equation (20) as

$$\frac{d}{dx}D = \frac{d}{dx}\left(D_0^2 - k_{evap}t\right)^{\frac{1}{2}} = \frac{1}{2}\left(D_0^2 - k_{evap}t\right)^{-\frac{1}{2}}\left(-k_{evap}\frac{dt}{dx}\right). \quad (26)$$

The kinematic derivative dt/dx can be replaced by $1/u(x,y)$, and within the differential control volume of length Δx, t can be approximated by $\Delta x/u(x,y)$. (For typical values of Δx, $D_0^2 \gg k_{evap}t$.) The dependence of k_{evap} on local temperature in the boundary layer is represented using the polynomial fit (equation 21). Equation (26) becomes

$$\frac{d}{dx}D = -\frac{1}{2}\left(D_0^2 - \frac{\left[A_1T^2 + B_1T + C_1\right]\Delta x}{u(x,y)}\right)^{-\frac{1}{2}}\left(\frac{A_1T^2 + B_1T + C_1}{u(x,y)}\right). \quad (27)$$

Substituting equations (25), (27), and (20) into equation (22) and simplifying, we obtain a dis-

[2] A linear profile is the simplest assumption that satifies these boundary conditions; however, the decreasing density is also expected because droplets nearer the fiber will move at higher axial speed, tending to lower particle concentrations. Given that integral solutions are not strongly sensitive to the profile shape assumed, and given that more detailed physical information about the number density profile is not currently available, we have chosen to use the simplest approximation.

cretized formulation of the integral

$$\int_0^{\delta_T} \dot{q}_e\,(a+y)dy\,\Delta x = -\int_0^{\delta_T} \frac{\pi\rho_w h_{fg} n_0 y(a+y)}{4\delta(x)}\left[A_1 T(x,y)^2 + B_1 T(x,y) + C_1\right] \times \left[D_0^2 - \frac{\left(A_1 T(x,y)^2 + B_1 T(x,y) + C_1\right)\Delta x}{u(x,y)}\right]^{\frac{1}{2}} dy\,\Delta x. \quad (28)$$

Numerical Solution

If the boundary layer temperature profile at any point on the fiber is known, then the heat transfer from the fiber can be calculated directly as

$$Q = -2\pi a k \left.\frac{\partial T}{\partial y}\right|_{y=o} \Delta x = -2\pi a k \left(\frac{-\Theta_f}{\beta a}\right)\Delta x = \frac{2\pi k \Theta_f}{\beta}\Delta x. \quad (29)$$

Hence, a knowledge of β can be used to calculate the axial fiber temperature distribution (*cf.*, equation 12). Equations (18) and (19) can be integrated from an initial α value to a final α value to obtain the β value at any position on the fiber. The initial condition on equation (18) is $\beta = 0$ at $\alpha = 0$, but this results in the equation being of an indeterminant form at $\alpha = 0$. To evaluate β for small values of α, a series expansion can be used in which β is approximated as

$$\beta = a_1\alpha + a_2\alpha^2 + a_3\alpha^3 + \cdots \quad (30)$$

with

$$a_1 = \frac{1}{2}\frac{(\mathrm{Pr}+2)}{\mathrm{Pr}} \quad (31)$$

$$a_2 = \frac{(\mathrm{Pr}-1)(\mathrm{Pr}+2)+4\eta}{9\ \mathrm{Pr}\ (\mathrm{Pr}+1)} \quad (32)$$

$$a_3 = \frac{(\mathrm{Pr}-1)(\mathrm{Pr}+2)(3\ \mathrm{Pr}^2 - 4\ \mathrm{Pr} - 2) + 60(3\ \mathrm{Pr}^2 + \mathrm{Pr} + 2)\eta + 360\eta^2}{270(\mathrm{Pr}+1)^2(3\ \mathrm{Pr}+2)} \quad (33)$$

In these relations, $\eta = (\rho c_p)/(\rho_f c_{p_f})$ as before; η is on the order of 10^{-3} for glass fibers in air. Equation (30) is used to evaluate β for α values from 0 to 0.08. The results from the series expansion are used as initial conditions for equation (18).

To obtain a solution to the fiber temperature profile along the length of the fiber, a Fehlberg fourth-fifth order Runge-Kutta method was used to forward integrate equations (18) and (19).

The evaporation integral (equation 28) also lacks a closed form solution and must be evaluated numerically. An adaptive Newton-Cotes method was used for the simulation. The integration step length of α was decreased until the fiber temperature profile coverged to within 1 K at 1 m. Decreasing the step length more than this would not change the fiber temperature profile by more than 1 K total no matter how much smaller the α increment was made, but decreasing the increment step further greatly increased the number of calculations and the simulation run time.

The simulation is designed to allow for initial spray induction to begin at any point x along the fiber; the spray is present from that location onward. Before the spray appears in the boundary layer, a no-spray solution is calculated by setting the spray density to zero. At the initial point of contact with the spray, the β value from the no-spray solution is used to determine the temperature profile. This profile is assumed constant over the small interval from α_i to α_{i+1}. This profile along with the corresponding x values are used to evaluate the evaporation integral. This numerical result is substituted back into the β differential equation which is then forward integrated to find β_{i+1}. With this value of β, the change in fiber temperature over Δx can be found using

$$\Delta T = \frac{-2\pi a k \left.\frac{\partial T}{\partial y}\right|_{y=0} \Delta x}{\pi a^2 \rho_f c_{p_f} U} = \frac{-2k\Theta_f}{a^2 \beta \rho_f c_{p_f} U} \Delta x \tag{34}$$

The fiber temperature at $x + \Delta x$ is simply $T_{x+\Delta x} = T_x + \Delta T$, and this value is then used as input to evaluate the evaporation term over the next interval. At each point, the α and β values are compared to determine which differential equation for β (18 or 19) should be used. This procedure is followed over the length of the fiber to solve for the fiber temperature profile.

The droplet diameter distribution at the beginning of any interval Δx is assumed uniform and equal to a specified SMD, representing the conditions in the air outside the boundary layer. Variable property effects are handled by using a local average film temperature and polynomial fits to tabulated data. The film temperature is changed for each successive increment of the fiber. This is in contrast to most published results for fiber cooling which have assigned a single property reference state along the entire length of the fiber.

Validation tests of the numerical model were performed in the limit of no spray. We ran calculations corresponding to the cases that were evaluated numerically and experimentally by Bourne and Dixon [6], with excellent agreement. As noted in the Introduction, subsequent studies of the no-spray situation have repeatedly confirmed the findings in [6].

Results

The numerical simulation has been run over a wide range of configurations, but for comparison purposes a baseline case was chosen: a 10 μm diameter fiber drawn at 60 m/s through still air at 320 K. The initial fiber temperature is 1500 K with a droplet density of 5000 drops/cm^3 and a representative Sauter mean diameter of 70 μm; these values are typical of the nozzles used in the industrial glass fiber forming process. The spray was injected into the fiber boundary layer at a distance $x = 1.8$ cm from the beginning of the fiber (corresponding to $\alpha = 5.0$). The baseline results for the no-spray and spray-cooled temperature profile are shown in Fig. 4. The sprayed fiber cools significantly more rapidly. For example, without spray the fiber reaches 400 K at $x = 1.2$ m, whereas with spray that temperature is reached at $x = 0.72$ m, a 40% reduction in distance. In terms of temperature differences, at a fiber position of $x = 1$ m the temperature difference between the spray cooled and no spray case is about 90 K (163°F).

Fiber temperature profiles were calculated using evaporation coefficients evaluated from both low and high rate mass transfer theory. Although the evaporation coefficients from the two theories vary significantly at high temperatures[3], the fiber cooling predictions of the two theories are almost identical. In the region of the boundary layer where the air temperatures are very high and high rate theory is essential, the total cross-sectional area is very small (proportional to $(y + a)^2$). The majority of the boundary layer volume is in the region where the temperatures are lower (T between 400 and 500 K) and the evaporation coefficients for the high and low rate theories are close. Most of the evaporative cooling takes place in this outer region of the boundary layer, and the evaporative cooling immediately adjacent to the fiber is very small owing to the small cross-sectional area and lower droplet density.

One of the primary control variables in the manufacturing process is the spray condition, specifically, the droplet size distribution and number density. The size distribution can be changed by changing nozzle types or by operating the nozzles at a different line pressure. The number density can be varied by changing the number of nozzles, changing the nozzle placement, changing the nozzle type, or changing the operating pressure. In Fig. 5, the droplet density varies from 0 to 10000 drops/cm^3 while the SMD is held constant. As the droplet density decreases, the temperature profile approaches the no spray profile. Conversely, as

[3]The values predicted by the two theories begin to diverge at about 500 K and differ by more than a factor of two at an air temperature 1500 K. Note that the water temperature is limited to values below 100°C at an ambient pressure of 1 atm.

number density increases, more liquid surface area is present and evaporative cooling effects are stronger.

Finer atomization of a given liquid volume produces stronger evaporative effects. Figure 6 shows the effect of reducing the SMD of a fixed volume of water per unit volume of air; this is equivalent to using successively finer atomizers at a fixed liquid flowrate. The spray volume used corresponds to baseline conditions of 5000 drops/cm^3 with an SMD of 70 μm. As SMD is decreased, the spray number density is increased to keep the ratio of water volume to total air volume constant. In the figure, as SMD decreases from 300 μm to 10 μm, the cooling of the fiber becomes progressively more rapid. The smaller the SMD, the more cooling for the same amount of water.

Figure 7 shows the thermal and momentum boundary layer thickness calculated with and without spray. As has been established by previous studies of long thin fibers, the boundary layer thickness may be more than two orders of magnitude greater than the fiber diameter. Spray cooling greatly thins the thermal boundary layer, and this causes a significant increase in the convective cooling of the fiber. The kink in the predicted boundary layer thickness with spray results from the assumption that the spray is instantaneously introduced at $x = 1.8$ cm. In reality, of course, the spray will require a certain distance to become distributed into the boundary layer.

The axial position at which the spray initially enters the boundary layer has an effect on the temperature profile. Figure 8 shows the fiber temperature profiles for spray entry points ranging from 1.8 cm below the bushing plate to 71 cm below the bushing plate. In terms of the fiber temperature beyond 90 cm from the bushing plate, it makes very little difference where the spray enters the boundary layer. This demonstrates that final fiber temperature is not sensitive to nozzle positioning along the fiber axis. If the objective is to simply cool the fiber before the point where the surfactant is applied, then getting spray into the fiber bundle and around each fiber is more important than having the spray contact each fiber at the same x position. If the physical properties or residual stress state of the fiber require a certain cooling rate between two particular temperatures, then vertical placement of the spray may become critical.

As the position of spray introduction is moved farther down the fiber, the thickness of the boundary layer into which the spray is injected becomes much greater. This in turn means that the cooling effect of the spray is greatly increased, since much more spray is contained

in a thicker boundary layer. That is the reason for the steeper cooling rates that occur in Fig. 8 when the spray is added far downstream of the bushing plate. Introducing the farther spray downstream also increases the numerical error in the calculations, owing to the much more abrupt change in the boundary layer growth rate immediately following the point of injection. Errors in the vicinity of the injection point affect the temperature profile along the remaining length of the fiber. In our calculations, when the spray was introduced very close to the beginning of the fiber (x = 1.8 cm), the numerical increment in α was decreased until the fiber temperature profile converged within 1 K. When the spray was introduced farther downstream, limitations in our computation led to errors of roughly 20 K at a distance x = 1 m; these errors contribute to the separation of the spray-cooled temperature profiles seen in Fig. 8.

The fiber cooling rates with and without spray are affected by the fiber size and drawing speed. Figure 9 shows the fiber temperature profile for a 10 μm fiber moving at 90 m/s. Spray conditions in this case are the same as the baseline, with a spray density of 5000 drops/m^3 and a SMD of 70 μm. Compared to the 10 μm fiber at 60 m/s (Fig. 4), the fiber temperature is reduced less over the same length of fiber. The opposite effect is seen for a fiber moving more slowly than the baseline condition. To illustrate the cooling of other sizes of fiber, Figure 10 shows the fiber temperature profile for a 25 μm fiber being drawn at 10 m/s. Spray cooling reduces the temperature at x = 1 m from 490 K to 370 K. Fig. 11 shows the temperature profile for a 5 μm fiber being drawn at 50 m/s. Spray cooling has much less of an effect on this small fiber. Without spray cooling, the fiber has already cooled to the final state value long before reaching 1 m. By x = 0.5 m, the fiber temperature is 320 K with spray cooling and 370 K without.

Summary and Recommendations

A model has been developed to describe the evaporative cooling of spun glass fibers by water sprays. This model can be used in designing and optimizing the spray processes used in glass fiber manufacturing.

The main implications of the model results are as follow. Spray cooling acts to thin the thermal boundary layers surrounding the fibers and to raise the convective heat removal from the fibers. The effectiveness of spray cooling can be increased by improving the atomization quality to give smaller droplets and by increasing droplet number density near the fibers. The

majority of the cooling takes place in the outer edges of a fiber's boundary layer. The vertical placement of the spray nozzles within the fiber bundle is a less critical parameter. The degree of spray cooling varies with fiber size and speed.

Three issues affecting the modeling of spray cooling require further study. The first is the turbulent transition of the boundary layer, which is ill-characterized in the existing literature. The second is the spray entrainment and dispersion within the axisymmetric fiber boundary layer, and, more generally, within the entire bundle of many hundreds of fibers. The last is the potential for droplet impact at high number density and high transverse droplet injection speeds. The present results are for laminar boundary layers in which droplets are evenly dispersed and travel at the local air speed and in which droplets do not directly interact with the fibers.

References

1. K.L. Loewenstein, *The Manufacturing Technology of Continuous Glass Fibres*, 3rd edn. Elsevier Science Publishers B.V., Amsterdam (1993).

2. R.A. Seban and R. Bond, Skin friction and heat transfer characteristics of a laminar boundary layer on a cylinder in axial incompressible flow, *J. Aeronautical Sci.* **18**, 671–675 (1951).

3. M.B. Glauert and M.J. Lighthill, The axisymmetric boundary layer on a long thin cylinder, *Proc. R. Soc. London* **A320**, 188–203 (1955).

4. B.C. Sakiadis, Boundary-layer behavior on continuous solid surfaces: III. The boundary layer on a continuous cylindrical surface, *AIChE Journal* **7**(3), 467–472 (1961).

5. D.E. Bourne and D.G. Elliston, Heat transfer through the axially symmetric boundary layer on a moving circular fibre, *Int. J. Heat Mass Transfer* **13**, 583–593 (1970).

6. D.E. Bourne and H. Dixon, The cooling of fibres in the formation process, *Int. J. Heat Mass Transfer* **24**, 1323–1332 (1971).

7. K. Chida and Y. Katto, Conjugate heat transfer of continuously moving surfaces, *Int. J. Heat Mass Transfer* **19**, 461–470 (1976).

8. J. Karniš and V. Pechoč, The thermal laminar boundary layer on a continuous surface, *Int. J. Heat Mass Transfer* **21**, 43–47 (1978).

9. R.E. Sayles, Approximate solution for the viscous boundary layer on a continuous cylinder, *AIChE Journal* **36**(12), 1917–1919 (1990).

10. E. Beese and K. Gersten, Skin friction and heat transfer on a circular cylinder moving in a fluid at rest, *J. Appl. Math. Physics* **30**, 117–127 (1979).

11. R.G.C. Arridge and K. Prior, Cooling time of silica fibers, *Nature* **203**, 386–387 (1964).

12. J.V. Alderson, J.B. Caress, and R.L. Sager, The cooling rate of glass fiber in the continuous filament process. Laboratory report No. L.R. 235 of Pilkington Bros. Ltd., Lathom, Lancashire, 1968.

13. R. Maddison and P.W. McMillan, The cooling rate of glass fibres, *Glass Technology* **19**(5), 127–129 (1978).

14. B.H. Kang, J. Yoo, and Y. Jaluria, Experimental study of the convective cooling of a heated continuously moving material, *J. Heat Transfer* **116**(1), 199–208 (1994).

15. E. Richelle, R. Tasse, and M.L. Riethmuller, Momentum and thermal boundary layer along a slender cylinder in axial flow, *Int. J. Heat Fluid Flow* **16**, 99–105 (1995).

16. S. Roy Choudhury and Y. Jaluria, Forced convective heat transfer from a continuously moving heated cylindrical rod in materials processing, *J. Heat Transfer* **116**(3), 724–734 (1994).

17. L.R. Glicksman, The cooling of glass fibres, *Glass Technology* **9**(5), 131–138 (1968).

18. *High-Speed Fiber Spinning* (Edited by A. Ziabicki and H. Kawai). Wiley, New York (1993).

19. N. Moussiopoulos, Numerical simulation of spray cooling pond performance, *J. Fluids Engr.* **109**, 179–185 (1987).

20. S.-J. Chen and A.A. Tseng, Spray and jet cooling in steel rolling, *Int. J. Heat Fluid Flow* **13**(4), 358–369 (1992).

21. W.M. Healy, P.J. Halvorson, J.G. Harley, and S.I. Abdel-Khalik, A critical heat flux correlation for droplet impact cooling at low Weber numbers and various pressures, *Int. J. Heat Mass Transfer* **41**, 975–978 (1998).

22. S.S. Kachhwaha, P.L. Dhar, and S.R. Kale, Experimental studies and numerical simulation of evaporative cooling of air with a water spray — I. Horizontal parallel flow, *Int. J. Heat Mass Transfer* **41**(2), 447–464, (1998).

23. S.S. Kachhwaha, P.L. Dhar, and S.R. Kale, Experimental studies and numerical simulation of evaporative cooling of air with a water spray — II. Horizontal counter flow, *Int. J. Heat Mass Transfer* **41**(2), 465–474 (1998).

24. F.P. Buckingham and A. Haji-Sheikh, Cooling of high temperature cylindrical surfaces using a water-air spray, *J. Heat Transfer* **117**(4), 1018–1027 (1995).

25. H. Papamichael and I.N. Miaoulis, Axial heat conduction effect in the cooling of optical fibres, *Glass Technology* **32**(3), 102–108 (1991).

26. M. Sweetland, Nozzle analysis and heat transfer model for spray cooling glass fibers, S.M. thesis, Massachusetts Institute of Technology, Cambridge, Masachusetts (1998).

27. A.H. Lefebvre, *Atomization and Sprays.* Hemisphere Publishing Corp., New York (1989).

28. A.F. Mills, *Heat and Mass Transfer.* R.D. Irwin, Boston (1995).

List of Figures

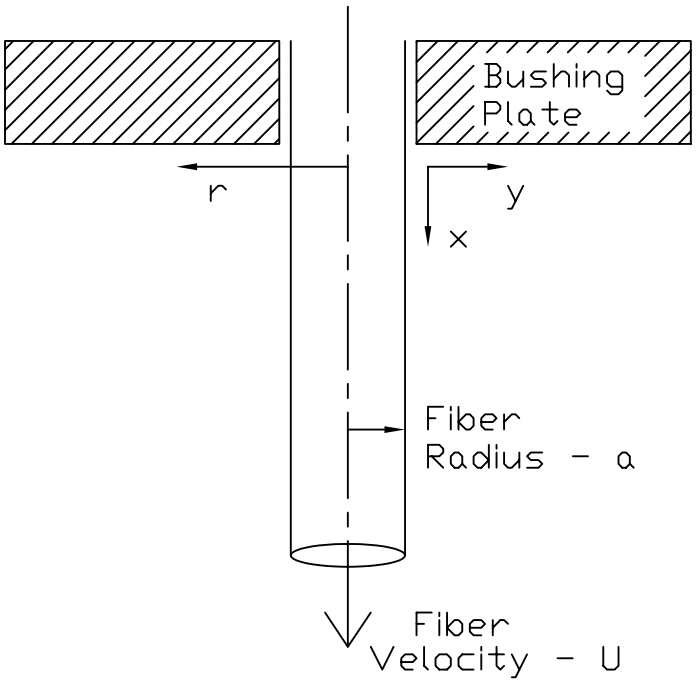

Figure 1: Coordinate system

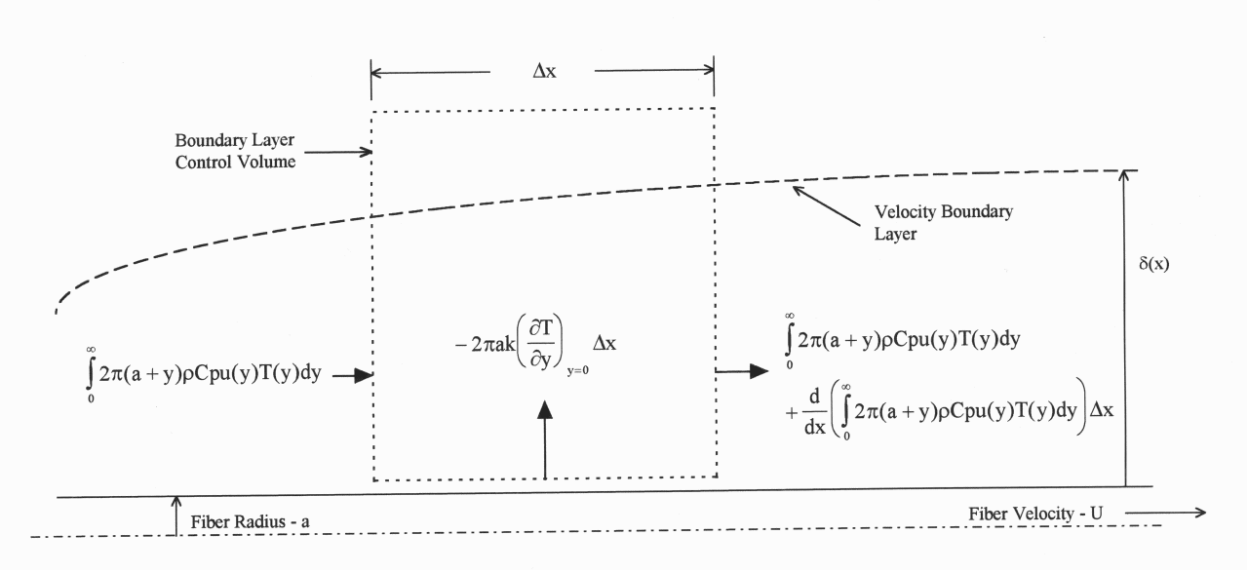

Figure 2: Boundary layer control volume.

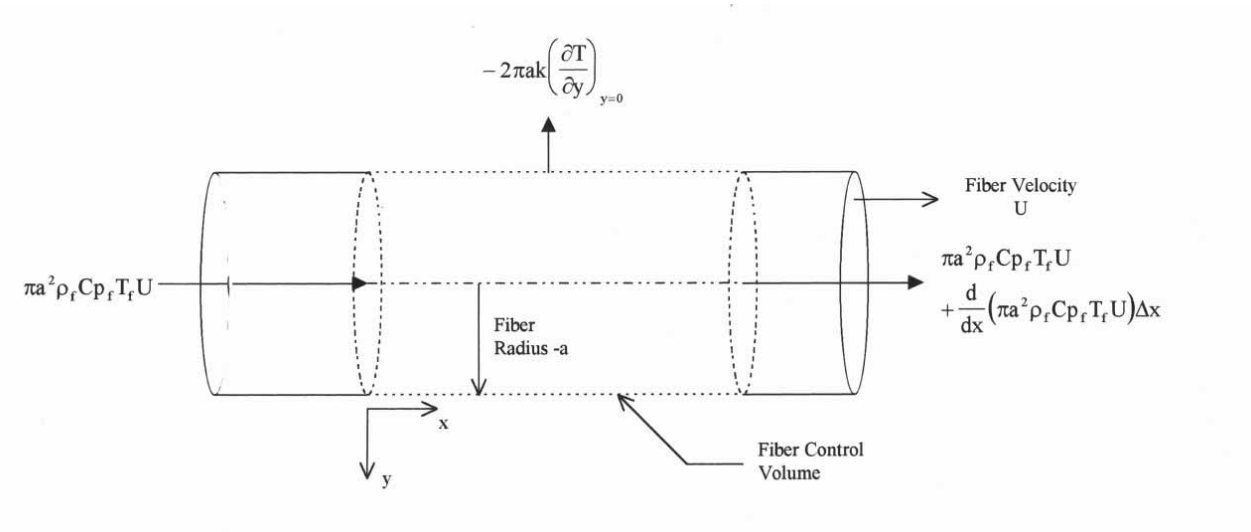

Figure 3: Fiber control volume

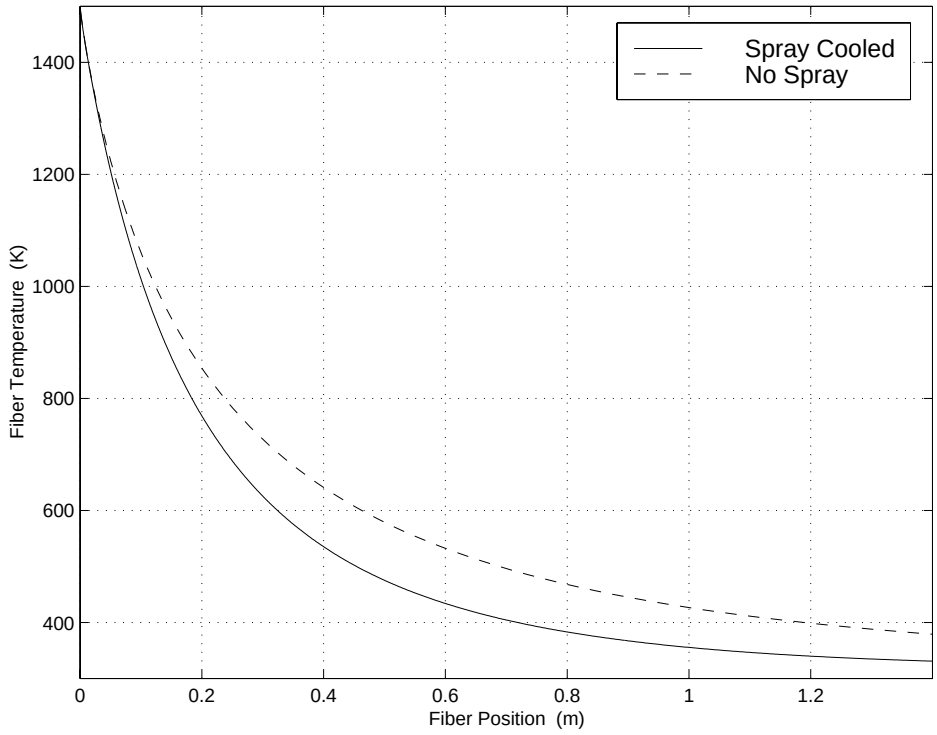

Figure 4: Baseline temperature profile for 10 μm fiber at 60 m/s.

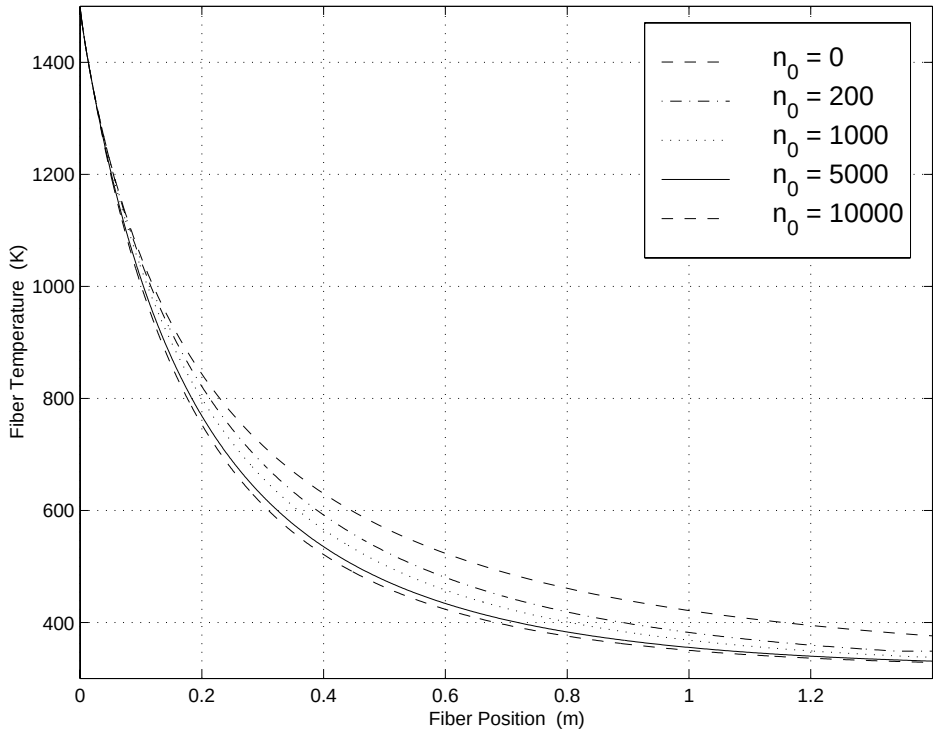

Figure 5: Temperature profile for varying droplet densities (SMD = 70 μm).

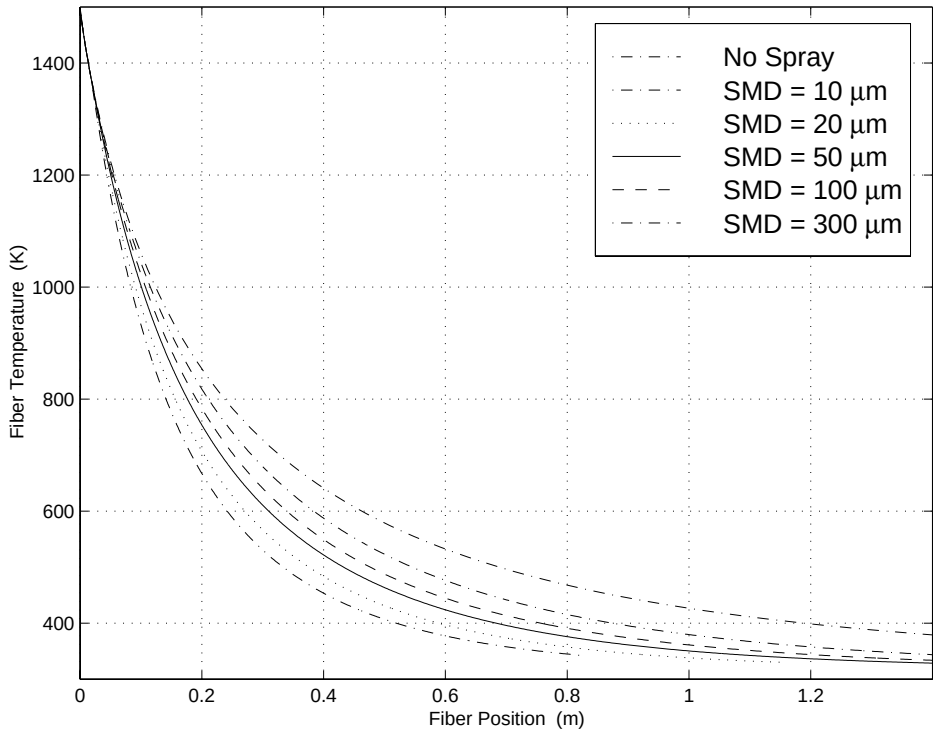

Figure 6: Temperature profiles for constant volume of sprayed liquid (9.0×10^{-4} m^3 water/m^3 air). The uppermost curve is for no spray and the lowermost is for an SMD of 10 µm.

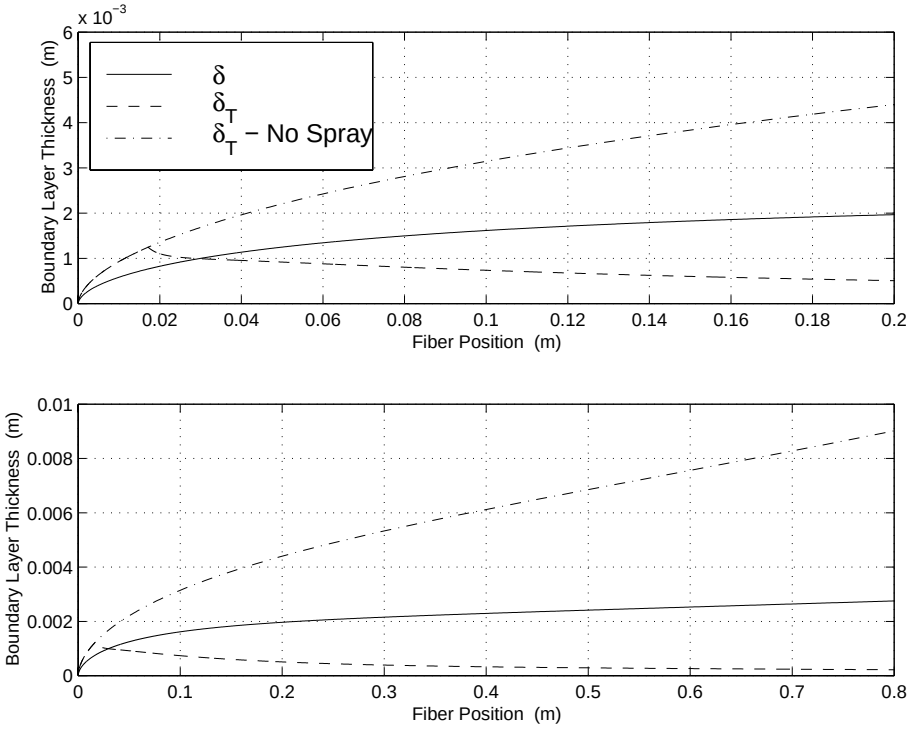

Figure 7: Thermal and velocity boundary layer thickness for baseline fiber conditions.

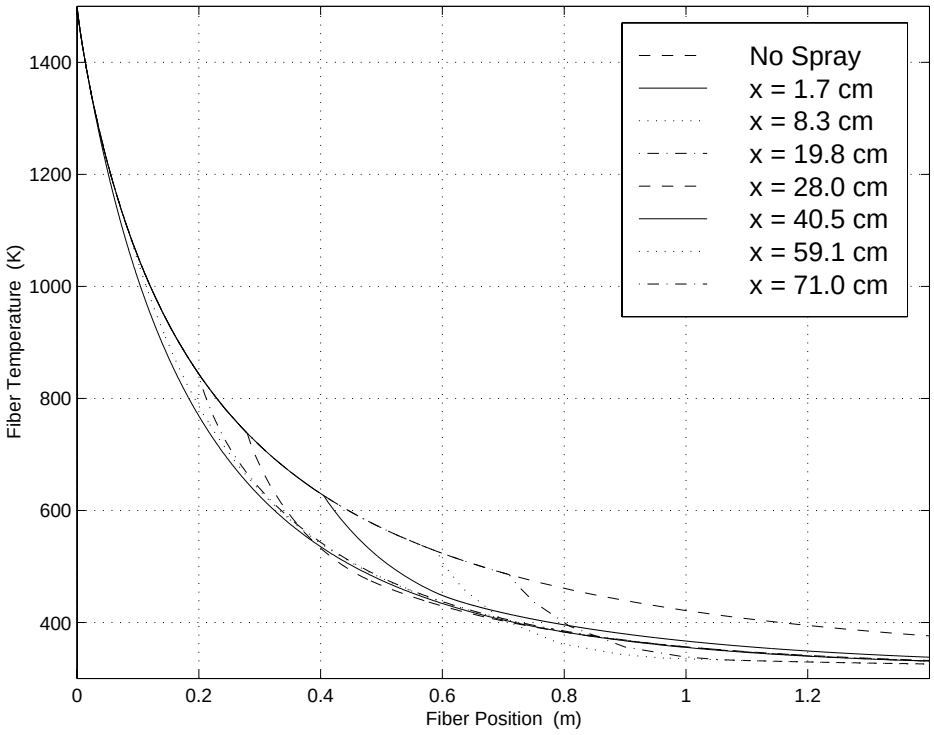

Figure 8: Temperature profiles for varying spray contact points.

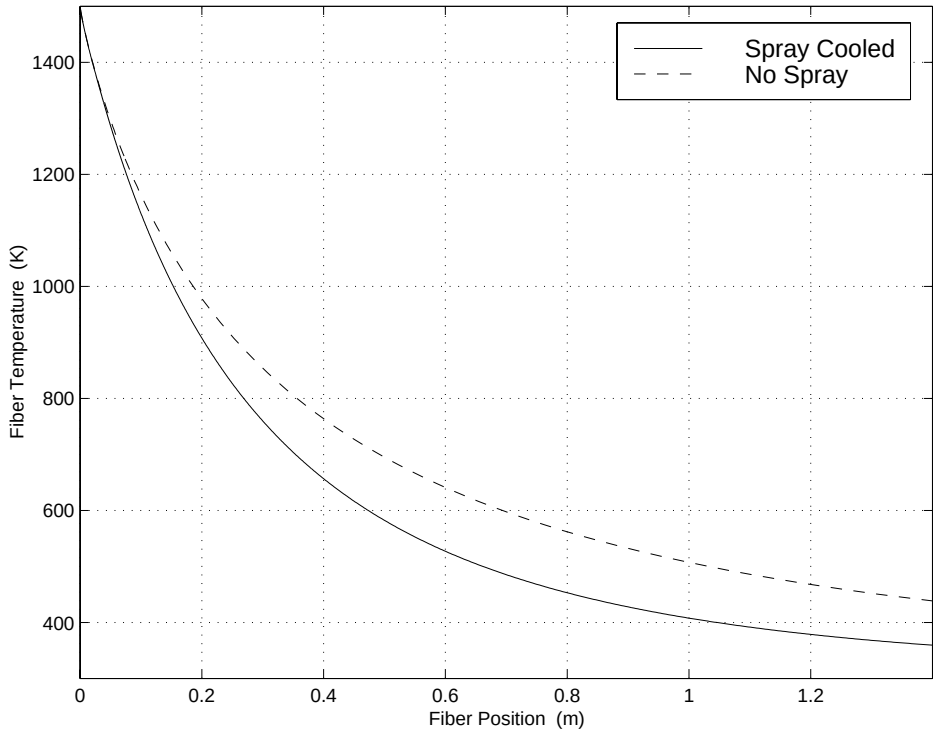

Figure 9: Fiber temperature profile for 10 μm fiber at 90 m/s.

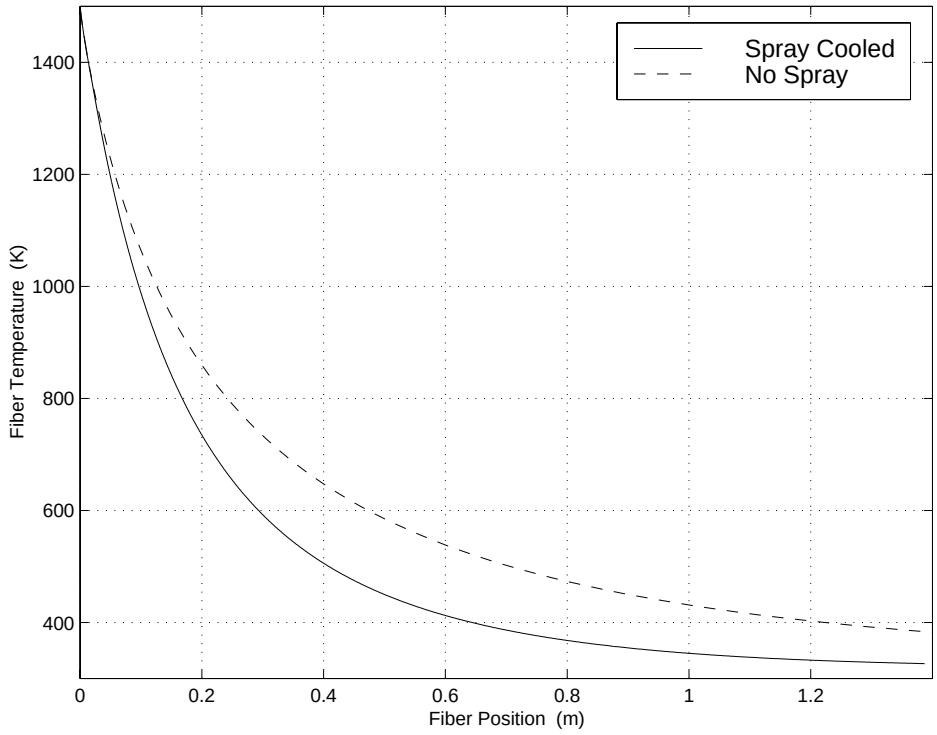

Figure 10: Fiber temperature profile for 25 μm fiber at 10 m/s.

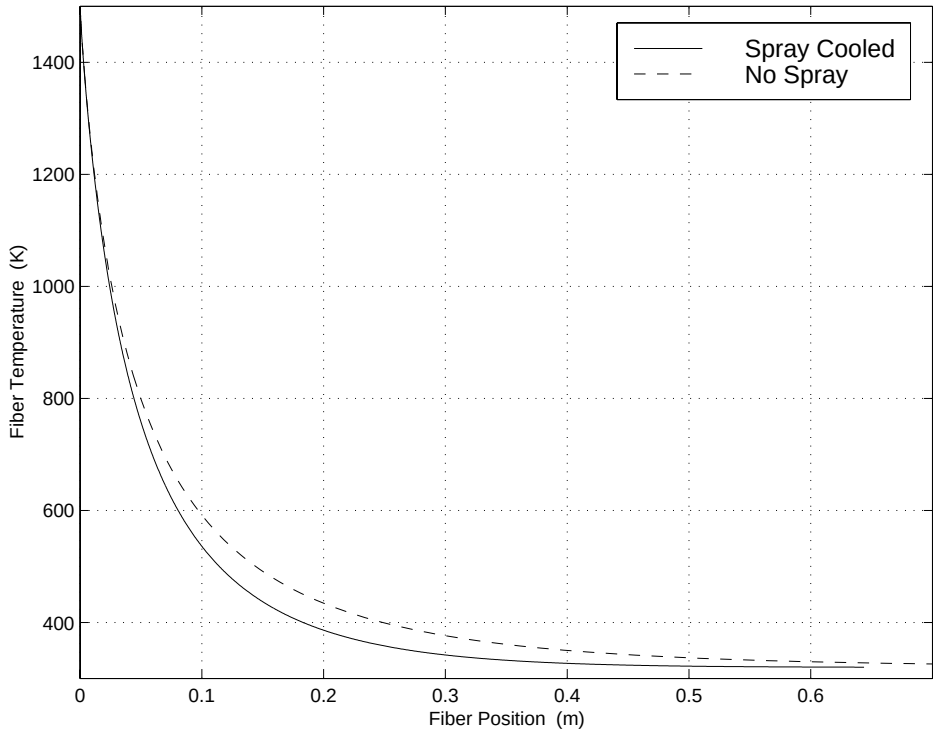

Figure 11: Fiber temperature profile for 5 μm fiber at 50 m/s.